

# Dual CNN Models for Unsupervised Monocular Depth Estimation

Vamshi Krishna Repala

Shiv Ram Dubey

Computer Vision Group,

Indian Institute of Information Technology, Sri City,  
Andhra Pradesh-517646, India

vamshi.r14, srdubey@iiits.in

## Abstract

*A lot of progress has been made to solve the depth estimation problem in stereo vision. Though, a very satisfactory performance is observed by utilizing the deep learning in supervised manner for depth estimation. This approach needs huge amount of ground truth training data as well as depth maps which is very laborious to prepare and many times it is not available in real scenario. Thus, the unsupervised depth estimation is the recent trend by utilizing the binocular stereo images to get rid of depth map ground truth. In unsupervised depth computation, the disparity images are generated by training the CNN with an image reconstruction loss based on the epipolar geometry constraints. The effective way of using CNN as well as investigating the better losses for the said problem needs to be addressed. In this paper, a dual CNN based model is presented for unsupervised depth estimation with 6 losses (DNM6) with individual CNN for each view to generate the corresponding disparity map. The proposed dual CNN model is also extended with 12 losses (DNM12) by utilizing the cross disparities. The presented DNM6 and DNM12 models are experimented over KITTI driving and Cityscapes urban database and compared with the recent state-of-the-art result of unsupervised depth estimation.*<sup>1</sup>

## 1. Introduction

The image based depth estimation of scene is a very active research area in the field of computer vision. Several researchers have shown their great interest to work over this problem due to its wide and real scenario applications [37] such as autonomous and assistive driving [26], [20], [7], human body pose estimation with 3D [34], robot assisted surgery [36], robot movement and grasping [19], learning human activities from RGBD videos [14], etc. The depth

map from images can be estimated in various ways like structure from motion [27], [39], multi-view stereo [33], [9], [5], monocular methods [30], [32], [23], single-image methods [31], [22], [4], etc. In early days, most of the image based depth estimation techniques were based on the key-point feature matching applied over multiple images of the scene of interest. Thus, the performance of such techniques was also compensated by hand-designed feature detection, description and matching approaches. In order to overcome these issues, the monocular depth estimation is treated as a supervised learning problem [4], [17], [23]. These supervised models predict the depth map for the monocular image corresponding to every pixel of the image. Such models are first trained in off-line mode with huge training database having monocular images as the inputs and corresponding depth maps as the labels. The limiting factor of these methods are the supervised training with huge amount of data and labels itself, which is not always available with the databases.

Nowadays, the deep learning and convolutional neural networks (CNNs) based methods perform outstanding in most of the problems of computer vision such as image classification [15], object detection [29], semantic segmentation [11], medical diagnosis [28], image retrieval [1], etc. Inspired from the success of deep learning, several researchers also tried to utilize the CNN framework for the image based depth prediction problem specially in monocular imaging conditions. These approaches are classified mainly in three categories namely learning-based stereo, supervised single view depth estimation and unsupervised depth estimation. The learning-based stereo methods learn dense correspondences [44], similarity measure on small image patches [42], stereo pairs extracted from 3D movies [40], classes as the possible disparities [24], contextual information using 3-D convolutions over geometry [13], etc. The stereo image pairs and ground truth disparity data are needed in order to train the learning-based stereo models. In real scenario, creating such data is very difficult. Moreover, these methods generally create the artificial data which can not

<sup>1</sup>Find the models and other information on the project GitHub page:

<https://github.com/ishmav16/>

Dual-CNN-Models-for-Unsupervised-Monocular-Depth-Estimation

represent the real challenges appearing in natural images and depth maps.

The supervised single view depth estimation methods also use ground truth depth to train the model. Eigen et al. used two deep networks for single view depth computation [4]. Their first network uses the entire image to perform a coarse global prediction, whereas second network locally rectify this prediction. The deep CNN and continuous conditional random field (CRF) are jointly used for single monocular image based depth estimation in deep convolutional neural field model [23]. Ladicky et al. refined the pixel-wise depth prediction problem into predicting only the likelihood of a pixel being at an arbitrarily fixed canonical depth to avoid the depth dependent training data bias [17]. A sequential deep network based on the cascade of multiple CRFs in CNN framework is used for the single-view depth training and estimation [41]. This method also fuses the complementary features extracted from multiple CNN side outputs. A fully convolutional architecture with up-sampling within the network is proposed by Liana et al. which utilizes the residual learning for estimating the depth map of a given single RGB image of a scene [18]. They also presented a suitable reverse Huber loss function for the said problem. The regression on deep convolutional neural network features is adapted by Li et al. to tackle the under-determined problem of depth and surface normal estimation from monocular images which uses CRF as a post-processing step for rectification [21]. The depth computation from single Image is treated as a classification problem with the help of deep fully convolutional residual Networks and a preprocessing step as fully-connected CRF for refinement [2]. Kuznetsov et al. [16] proposed a semi-supervised approach by training the CNN with supervised and unsupervised depth information. The ground truth depth information is captured through a 3D laser camera for supervised labels. The main hurdle in supervised approaches is availability and creation of ground truth depth maps which is always not available in real scenario applications.

In order to overcome the limitations of aforementioned supervised depth estimation techniques, some researchers have started working for unsupervised depth estimation which works reasonably good as well comparable to the supervised methods without need of any ground truth depth maps. The unsupervised methods utilize the underlying theory of epipolar constraints [10]. Recently, Garg et al. used auto-encoder deep CNN to predict the inverse depth map (i.e. disparity) from left image [6]. They computed a warp image (i.e. reconstructed left image) from disparity map and right image. Finally, the error between original and reconstructed left image is used as the loss to train the whole setup in unsupervised manner. This approach is further improved by Godard et al. by incorporating the left-right consistency [8]. In left-right consistency, basically two depth

maps (i.e. left and right) are generated using auto-encoder only from the left input image. The left input image is used with generated right depth map and the right image is used with generated left depth map to reconstruct the right and left images respectively. Zhou et al. [43] utilized the concepts of unsupervised image depth estimation proposed in [4] and [8] to tackle the monocular depth and camera motion estimation in unstructured video sequences in unsupervised learning framework. In one of the recent work, the 3D loss such as photometric quality of frame reconstructions is combined with 2D loss such as pixel-wise or gradient-based loss for learning the depth and ego-motion from monocular video in unsupervised manner [25].

While the unsupervised based methods have gained the attention in recent times due to non-requirement of ground truth depth maps, there is still need of discovering better suited unsupervised networks and loss functions. Through this paper, we propose a dual CNN based model for unsupervised monocular image depth estimation by utilizing the 6 losses (DNM6). We also extend the dual CNN model with 12 losses and generate DNM12 architecture to improve the quality of depth maps. The losses used in this paper are the appearance matching loss, disparity smoothness loss and left-right consistency loss.

The rest of the paper is structured by presenting the proposed dual CNN models in Section 2, the experimental setup in Section 3, the results and analysis in Section 4, and the concluding remarks in Section 5.

## 2. Proposed Methodology

Recently Garg et al. [6] approached the unsupervised depth estimation problem using CNN which is further improved by Godard et al. [8] by introducing a left-right consistency loss. These methods only need the monocular images for training without any ground truth depth maps. Inspired from [6] and [8], we propose the dual CNN models (DNM6 and DNM12) for unsupervised depth estimation which further improves these works.

### 2.1. Dual Network Model with 6 Losses (DNM6)

The proposed idea of dual network model (DNM) using CNN is illustrated in Figure 1. This model is based on the 6 losses, thus referred as the DNM6 model. The DNM6 model has two CNN one for each left and right images of stereo pair. During training, the left image  $I^l$  and right image  $I^r$  are considered as the inputs to the left CNN named as CNN-L and right CNN named as CNN-R respectively. The  $I_{i,j}$  refers to the  $(i, j)^{th}$  co-ordinate of image  $I$ . It is assumed that both  $I^l$  and  $I^r$  images are captured in similar settings. Both CNN's are based on the auto-encoder algorithm and combined these two networks named as dual network. The CNN architecture (in both CNNs) is taken from the Godard et al. [8]. The CNN-L predicts the left disparity

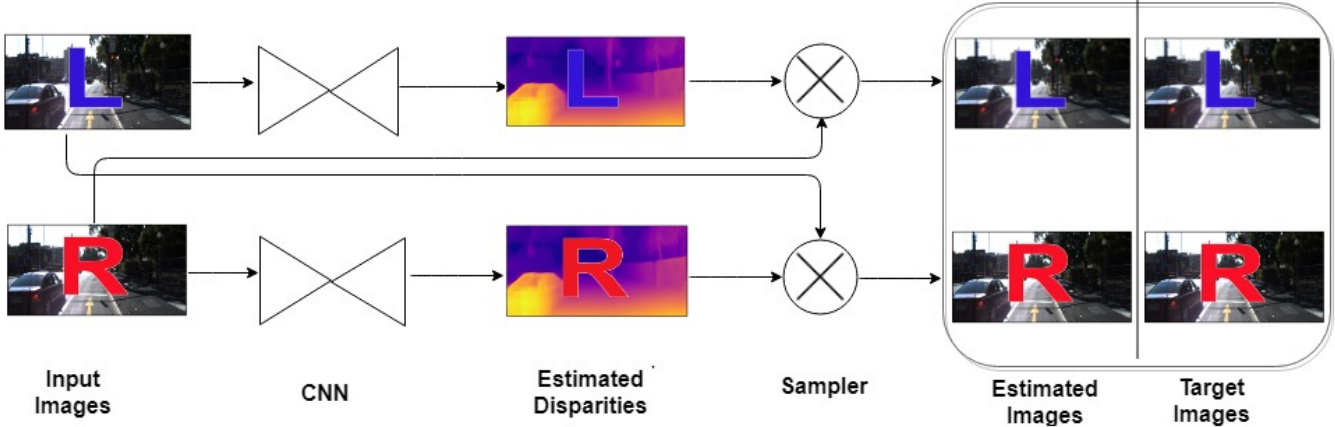


Figure 1. Pictorial representation of proposed Dual Network Model with 6 Losses (DNM6)

map  $d^l$ , whereas the CNN-R predicts the right disparity map  $d^r$ . The  $d_{i,j}$  refers to disparity value at  $(i, j)^{th}$  co-ordinate of disparity map  $d$ . In order to reconstruct the left and right image from left and right disparity maps ( $d^l$  and  $d^r$ ), the bi-linear sampling from the Spatial Transform Networks [12] is used in this paper. The similar approach is also followed in [8] for reconstruction from disparity map. The left image is reconstructed from the left disparity map  $d^l$  and input right image  $I^r$ , whereas the right image is reconstructed from the right disparity map  $d^r$  and input left image  $I^l$  as shown in the Figure 1. The reconstructed left and right images are referred as  $\hat{I}^l$  and  $\hat{I}^r$  respectively throughout the paper. We also used the loss functions ( $C$ ) such as appearance matching loss ( $C_{ap}$ ), disparity smoothness loss ( $C_{ds}$ ) and left-right consistency loss ( $C_{lr}$ ) similar to [8] but in dual network framework. The loss functions are defined below.

**Appearance Matching loss:** To enforce the appearance of estimated images must be similar to the input image, a combination of L1 norm and Structural Similarity Index Metric (SSIM) [38] loss term is used for both left and right images which is defined as follows [8],

$$C_{ap}^\beta = \frac{1}{N} \sum_{i,j} \alpha \frac{1 - SSIM(I_{ij}^\beta, \hat{I}_{ij}^\beta)}{2} + (1-\alpha) \| I_{ij}^\beta - \hat{I}_{ij}^\beta \| \quad (1)$$

where  $\beta \in \{l, r\}$ ,  $C_{ap}^l$  refers appearance matching loss between estimated left image and input left image and  $C_{ap}^r$  refers appearance matching loss between estimated right image and input right image and  $\alpha$  represents the weight between SSIM and L1 norm.

**Disparity Smoothness Loss:** The image gradient based disparity smoothness loss is computed from both disparity maps to ensure the estimated disparity map should be smooth. Similar to [8], the disparity smoothness loss is given by the following equations,

$$C_{ds}^\beta = \frac{1}{N} \sum_{i,j} |\partial_x d_{ij}^\beta| e^{-\|\partial_x I_{ij}^\beta\|} + |\partial_y d_{ij}^\beta| e^{-\|\partial_y I_{ij}^\beta\|} \quad (2)$$

where  $\beta \in \{l, r\}$ ,  $C_{ds}^l$  refers the disparity smoothness loss of left disparity map  $d^l$  estimated by CNN-L,  $C_{ds}^r$  refers the disparity smoothness loss of right disparity map  $d^r$  estimated by CNN-R and  $\partial$  is the partial derivative.

**Left Right Consistency Loss:** To maintain the estimated left disparity map  $d^l$  and right disparity map  $d^r$  to be consistent, the L1 term penalties on estimated disparities similar to [8] are computed between  $d^l$  and  $d^r$  as follows,

$$C_{lr} = \frac{1}{N} \sum_{i,j} |d_{ij}^l - d_{ij+d_{ij}^l}^r| \quad (3)$$

and

$$C_{rl} = \frac{1}{N} \sum_{i,j} |d_{ij}^r - d_{ij+d_{ij}^r}^l| \quad (4)$$

where  $C_{lr}$  and  $C_{rl}$  refer the left to right and right to left consistency losses respectively.

Similar to Godard et al. [8], four output scales  $s$  in both left and right CNNs are used in this paper in order to make the loss functions more robust. The combined cost function  $C_s$  at scale  $s$  including all above losses i.e. appearance matching losses  $C_{ap}^l$  and  $C_{ap}^r$ , disparity smoothness losses  $C_{ds}^l$  and  $C_{ds}^r$  and left-right consistency losses  $C_{lr}$  and  $C_{rl}$  is given as  $C_s = \alpha_{ap}(C_{ap}^l + C_{ap}^r) + \alpha_{ds}(C_{ds}^l + C_{ds}^r) + \alpha_{lr}(C_{lr} + C_{rl})$ . The final Cost/Loss function for proposed DNM6 model is computed as  $C = \sum_{s=1}^4 C_s$  at different output scales from  $s = 1$  to 4 similar to [8]. At testing time, a single left image,  $I^l$  is needed as the input to the left CNN (i.e., CNN-L) and it predicts the disparity map  $d^l$  from the trained network. Note that, the right CNN with input  $I^r$  can also be used to predict the disparity map  $d^r$ . Once disparity map  $d$  (i.e.  $d^l$  or  $d^r$ ) is computed, it can be converted into

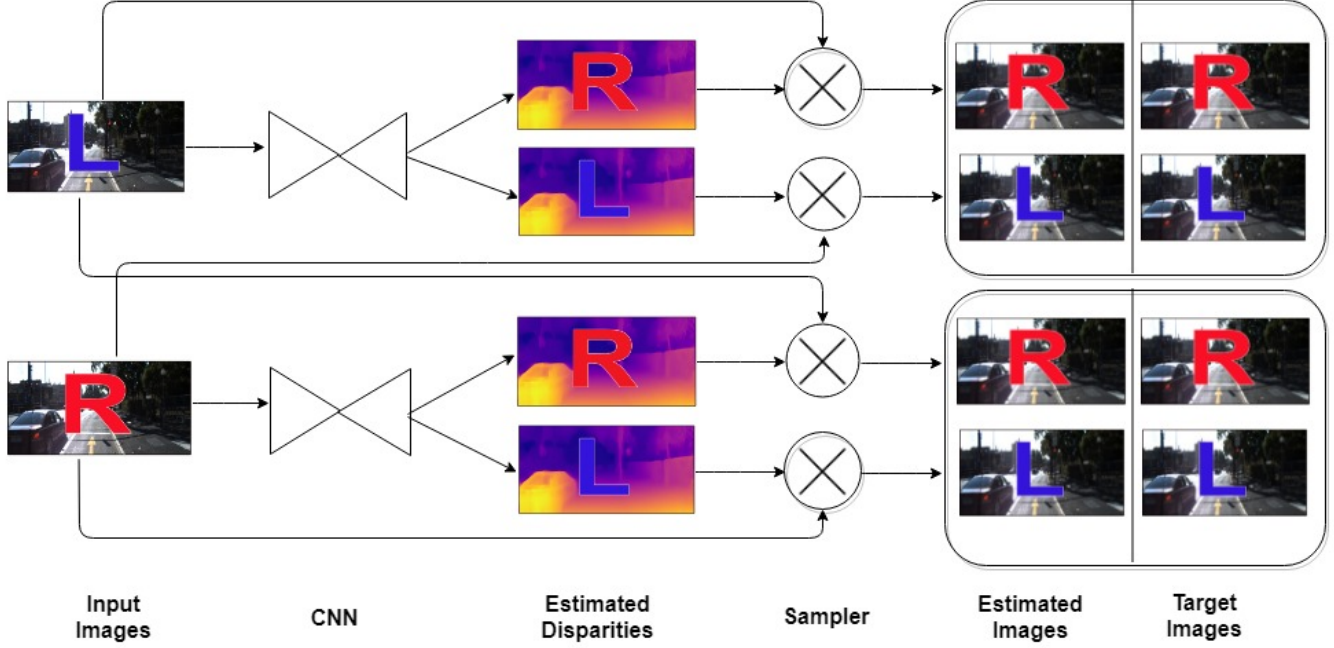


Figure 2. Pictorial representation of our Dual Network Model with 12 losses (DNM12)

depth map ( $D$ ) as  $D = \frac{f \times B}{d}$ , where  $f$  represents the focal length and  $B$  is the baseline between stereo cameras.

## 2.2. Dual Network Model with 12 Losses (DNM12)

In our previous DNM6 model, disparity maps are estimated from each network individually, whereas in this DNM12 model, the left-right cross disparity mapping is also proposed as depicted in Figure 2. The left and right CNN networks of DNM6 are extended to generate two output disparities (i.e. left and right) from each CNN. Similar to Godard et al. [8], it generates both left and right disparity maps from a single image. During training, the left image  $I^l$  and right image  $I^r$  of stereo pair are provided as inputs to the left CNN (CNN-L) and right CNN (CNN-R) respectively. In DNM12 architecture, both the CNN's predict the left and right disparities independently as illustrated in Figure 2. Here, we consider  $d^{l_L}$  and  $d^{l_R}$  as the left and right disparity maps respectively estimated by the left CNN-L and similarly  $d^{r_L}$  and  $d^{r_R}$  as the left and right disparity maps respectively estimated by the right CNN-R. As shown in the Figure 2, four bilinear samplers are used for reconstructing the two output left images  $\hat{I}^{l_L}$  and  $\hat{I}^{l_R}$  corresponding to left input image and two output right images  $\hat{I}^{r_L}$  and  $\hat{I}^{r_R}$  corresponding to right input image. The  $\hat{I}^{l_L}$  uses  $d^{l_L}$  and  $I^r$ ,  $\hat{I}^{l_R}$  uses  $d^{l_R}$  and  $I^l$ ,  $\hat{I}^{r_L}$  uses  $d^{r_L}$  and  $I^r$ , and  $\hat{I}^{r_R}$  uses  $d^{r_R}$  and  $I^l$ . Due to cross CNN mapping, the number of losses ( $C$ ) is doubled in DNM12 as compared to our previous DNM6 model. In DNM12, four appearance matching losses, four disparity smoothness losses and four left-right consistency

losses are considered from the two left and right networks.

The *Four Appearance Matching Losses* are defined as follows,

$$C_{ap}^{\beta\gamma} = \frac{1}{N} \sum_{i,j} \alpha \frac{1 - SSIM(I_{ij}^{\gamma}, \hat{I}_{ij}^{\beta\gamma})}{2} + (1-\alpha) \| I_{ij}^{\gamma} - \hat{I}_{ij}^{\beta\gamma} \| \quad (5)$$

where  $\beta \in \{l, r\}$ ,  $\gamma \in \{l, r\}$ ,  $C_{ap}^{l_L}$  and  $C_{ap}^{l_R}$  are the appearance matching losses for left CNN-L and  $C_{ap}^{r_L}$ ,  $C_{ap}^{r_R}$  are the appearance matching losses for right CNN-R. The total appearance matching loss is given by  $C_{ap} = (C_{ap}^{l_L} + C_{ap}^{l_R} + C_{ap}^{r_L} + C_{ap}^{r_R})$ .

The *Four Disparity Smoothness Losses* are computed as follows,

$$C_{ds}^{\beta\gamma} = \frac{1}{N} \sum_{i,j} |\partial_x d_{ij}^{\beta\gamma}| e^{-\|\partial_x I_{ij}^{\beta}\|} + |\partial_y d_{ij}^{\beta\gamma}| e^{-\|\partial_y I_{ij}^{\beta}\|} \quad (6)$$

where  $\beta \in \{l, r\}$ ,  $\gamma \in \{l, r\}$ ,  $C_{ds}^{l_L}$ ,  $C_{ds}^{l_R}$  are the disparity smoothness losses for left CNN-L and  $C_{ds}^{r_L}$ ,  $C_{ds}^{r_R}$  are the disparity smoothness losses for right CNN-R. The total disparity smoothness loss is computed as  $C_{ds} = (C_{ds}^{l_L} + C_{ds}^{l_R} + C_{ds}^{r_L} + C_{ds}^{r_R})$ .

The *Four Left-Right Consistency Losses* are calculated as follows,

$$C_{lr}^l = \frac{1}{N} \sum_{i,j} |d_{ij}^{l_L} - d_{ij+d_{ij}^{l_L}}^{l_R}|, \quad (7)$$

$$C_{rl}^l = \frac{1}{N} \sum_{i,j} |d_{ij}^{l_R} - d_{ij+d_{ij}^{l_R}}^{l_L}|, \quad (8)$$

$$C_{lr}^r = \frac{1}{N} \sum_{i,j} |d_{ij}^{r_l} - d_{ij+d_{ij}^{r_l}}^{r_r}|, \quad (9)$$

and

$$C_{rl}^r = \frac{1}{N} \sum_{i,j} |d_{ij}^{r_r} - d_{ij+d_{ij}^{r_l}}^{r_l}| \quad (10)$$

where  $C_{lr}^l$ ,  $C_{rl}^l$  are the left-right and right-left consistency losses for left CNN-L and  $C_{lr}^r$ ,  $C_{rl}^r$  are the left-right and right-left consistency losses for right CNN-R. The total left-right consistency loss is calculated as  $C_{lr} = (C_{lr}^l + C_{rl}^l + C_{lr}^r + C_{rl}^r)$ .

Similar to DNM6, the total Loss function in DNM12 is also defined as  $C = \sum_{s=1}^4 C_s$  at different output scales from  $s = 1$  to 4, where  $C_s$  at a particular scale is computed by weighted sum of all losses as follows,

$$C_s = \alpha_{ap} \times C_{ap} + \alpha_{ds} \times C_{ds} + \alpha_{lr} \times C_{lr}. \quad (11)$$

The same procedure as provided in previous DNM6 model is followed in DNM12 also for testing, a single image is taken as input to either CNN-L or CNN-R and it predicts the disparity map from the trained network which is converted into depth map.

### 3. Experimental Setup

#### 3.1. About Dataset

We used the standard datasets such as KITTI Stereo 2015 [7] and Cityscapes Urban Scene 2016 [3] for the experiments. The KITTI database [7] consists of 42,382 stereo pairs from different scenes. Out of them, 29,000 stereo pairs are used for training similar to [8]. From the official KITTI dataset, 200 high-quality images are released as the test cases along with its depth maps which is used in this paper for the evaluation and comparison. The same test images and its depth maps as ground truths are also considered by Godard et al. [8]. The Cityscapes database [3] contains 22,973 stereo pairs which are captured for autonomous driving in an urban environment of 50 cities scenes across the country Germany involving high inner city street scenes. Compared to KITTI database, the Cityscapes database images are of high resolution and better quality. Similar to Godard's work [8], we have also used the whole 22,973 stereo pairs for training after cropping each image such that the 80% of the height is preserved and the car hoods are removed. The DNM6 and DNM12 models are trained over full Cityscapes database and evaluated on the same 200 standard KITTI stereo images which are used to evaluate the performance over KITTI database.

#### 3.2. Implementation Details

The CNN architectures in our network are same as in Godard et al. [8] applied in dual CNN framework. It is based

on the auto-encoder concept consisting of the encoder as a variant of VGG16 [35] and decoder. The encoder consists of the 14 convolutional layers and converts the 3 input image channels into 512 channel map similar to Godard et al. [8]. The decoder consists of the 7 up-convolutional layers, 7 merging layers and 4 disparity layers similar to Godard et al. [8]. This network is implemented in TensorFlow which contains 62 million trainable parameters including weights and biases and trained by using NVIDIA Tesla K80 24GB GDDR5 GPU server up to 50 epochs which took 49 hours over KITTI database for the following parameters,  $\alpha = 0.85$ ,  $\alpha_{ap} = 1$ ,  $\alpha_{ds} = 0.1$ ,  $\alpha_{lr} = 1.0$  and learning rate  $\lambda = 10^{-4}$  for first 30 epochs and  $0.5 \times 10^{-4}$  for next 10 epochs and  $0.25 \times 10^{-4}$  for the last 10 epochs. The data augmentation is done on fly in similar way by following the Godard et al. [8] including flipping and color augmentations. During test time, a post-processing is performed to reduce the effect of stereo dis-occlusions similar to [8].

## 4. Experimental Results

In this section, first the evaluation criteria is presented in terms of the used evaluation metrics for depth estimation and then the depth estimation results are discussed over KITTI driving and Cityscapes urban databases using these evaluation measures.

#### 4.1. Evaluation Criteria

We considered the 200 high-quality images provided from the official KITTI driving dataset as input to our trained networks and estimated the corresponding disparity maps in both methods. In both DNM6 and DNM12 methods, these estimated disparity maps  $d(x)$  are further converted into depth maps as  $D(x) = \frac{fB}{d(x)}$ , where  $f$  is the focal length of camera and  $B$  is the baseline distance between both camera in stereo setup. The evaluation of both models are done with the estimated depth maps  $D(x)$  and provided ground truth depth maps  $G(x)$ . The evaluation metrics are same as in [4], [8] such as Absolute Relative difference (**Abs Rel**), Squared Relative difference (**Sq Rel**), Root Mean Square Error (**RMSE**), **RMSE log**, **d1-all** defined as follows,

$$\text{Abs Rel} = \frac{1}{n} \sum_{i=1}^n \frac{|G(x_i) - D(x_i)|}{G(x_i)}, \quad (12)$$

$$\text{Sq Abs} = \frac{1}{n} \sum_{i=1}^n \frac{|G(x_i) - D(x_i)|^2}{G(x_i)}, \quad (13)$$

$$\text{RMSE} = \sqrt{\frac{1}{n} \sum_{i=1}^n (G(x_i) - D(x_i))^2}, \quad (14)$$

$$\text{d1-all (\%)} = \frac{1}{n} \sum \text{bad pixels} \times 100, \quad (15)$$

Table 1. Experimental results by using proposed dual CNN based DNM6 and DNM12 models for unsupervised depth estimation over KITTI benchmark database. The training is done over KITTI training images and the evaluation is done over KITTI test images. In this table, pp denotes the post-processing. The best results without post-processing are highlighted in bold face.

Method	Lower is better					Higher is better		
	Abs Rel	Sq Rel	RMSE	RMSE log	d1-all	<b>a1</b>	<b>a2</b>	<b>a3</b>
Godard et al. [8] No LR	0.123	1.417	6.315	0.220	30.318	0.841	0.937	0.973
Godard et al. [8]	0.124	1.388	6.125	0.217	<b>30.272</b>	0.841	0.936	0.975
DNM6 Model	0.1223	1.4004	6.162	0.214	31.050	<b>0.848</b>	<b>0.941</b>	<b>0.976</b>
DNM12 Model	<b>0.1221</b>	<b>1.3058</b>	<b>6.069</b>	<b>0.213</b>	31.455	0.841	0.939	<b>0.976</b>
DNM6 Model PP	0.1157	1.2037	5.830	0.203	30.004	0.852	0.945	0.979
DNM12 Model PP	0.1157	1.1404	5.772	0.203	30.342	0.848	0.944	0.979

Table 2. Experimental results by using proposed dual CNN based DNM6 and DNM12 models for unsupervised depth estimation over Cityscapes benchmark database. The training is done over Cityscapes training images and the evaluation is done over KITTI test images. In this table, pp denotes the post-processing. The best results without post-processing are highlighted in bold face.

Method	Lower is better					Higher is better		
	Abs Rel	Sq Rel	RMSE	RMSE log	d1-all	<b>a1</b>	<b>a2</b>	<b>a3</b>
Godard et al. [8]	0.699	10.060	14.445	0.542	94.757	0.053	0.326	0.862
DNM6 Model	0.2704	3.7637	9.186	0.326	64.215	0.649	0.864	0.941
DNM12 Model	<b>0.2661</b>	<b>3.6491</b>	<b>8.915</b>	<b>0.316</b>	<b>61.163</b>	<b>0.669</b>	<b>0.875</b>	<b>0.946</b>
DNM6 Model PP	0.2474	2.9781	8.406	0.300	63.780	0.663	0.881	0.954
DNM12 Model PP	0.2396	2.8945	8.178	0.289	58.733	0.687	0.889	0.959

and

$$\text{RMSE log} = \sqrt{\frac{1}{n} \sum_{i=1}^n (\log G(x_i) - \log(D(x_i))^2} \quad (16)$$

where bad pixels are those pixels which satisfy the following two conditions  $|g(x_i) - d(x_i)| \geq 3$  and  $|g(x_i) - d(x_i)|/G(x_i) \geq 0.05$ , where  $g(x_i) = \frac{fB}{G(x_i)}$  is the ground truth disparity map computed from the ground truth depth map  $G(x_i)$  and  $d(x_i)$  is the predicted disparity map. The lower values of these metrics represent the better performance. We also measured the *Accuracy metrics* for which higher is better. Consider  $\delta_i$  is the threshold value for the pixel  $i$  as  $\delta_i = \max(\frac{G(x_i)}{D(x_i)}, \frac{D(x_i)}{G(x_i)})$ , then the three metrics (**a1**, **a2**, and **a3**) are defined as **a1** =  $\frac{1}{n} \times \text{No. of pixels having } \delta < 1.25$ , **a2** =  $\frac{1}{n} \times \text{No. of pixels having } \delta < (1.25)^2$ , and **a3** =  $\frac{1}{n} \times \text{No. of pixels having } \delta < (1.25)^3$  respectively, where  $n$  is the no. of pixels in the ground truth depth map (or) estimated depth map.

## 4.2. Results

The proposed DNM6 and DNM12 models are used for the unsupervised monocular depth estimation over benchmark KITTI driving database. The results in terms of the **Abs Rel**, **Sq Rel**, **RMSE**, **RMSE log**, **d1-all** as well as the accuracies at different thresholds (i.e. **a1**, **a2**, and **a3**) are reported in Table 1 over KITTI database. The results of pro-

posed DNM6 and DNM12 models are also compared with very recent state-of-the-art unsupervised method proposed by Godard et al. [8] with and without left-right (LR) consistency in Table 1. Note that the lower values of **Abs Rel**, **Sq Rel**, **RMSE**, **RMSE log**, and **d1-all** and the higher values of accuracies **a1**, **a2**, and **a3** represent the better performance. The performance of proposed DNM6 and DNM12 methods are also tested with a pre-procesing (**PP**) step to reduce the effect of stereo dis-occlusions [8].

The best results without PP are highlighted in bold face in Table 1. It can be easily observed that the proposed dual CNN based models i.e. both DNM6 and DNM12 perform better than Godard et al. [8] with and without left-right consistency. The **Abs Rel**, **Sq Rel**, **RMSE**, **RMSE log**, and **d1-all** values are generally lower and accuracies **a1**, **a2**, and **a3** are higher for the proposed DNM6 and DNM12 methods. It is also noticed that DNM12 completely outperforms the Godard et al. [8] in all terms except **d1-all**. The performance of DNM6 model is improved in terms of the **Abs Rel**, **RMSE**, **a1**, **a2**, and **a3** as compared to the Godard model. The DNM12 model exhibits the better performance as compared to the DNM6 model in all terms except accuracies. As for as accuracies are concerned, the DNM6 model is superior as compared to DNM12 model because generating right disparity from left image and left disparity from right image is not suited for pixel level thresholding. This is also seen that the performance of proposed models improved significantly with post-processing step over KITTI

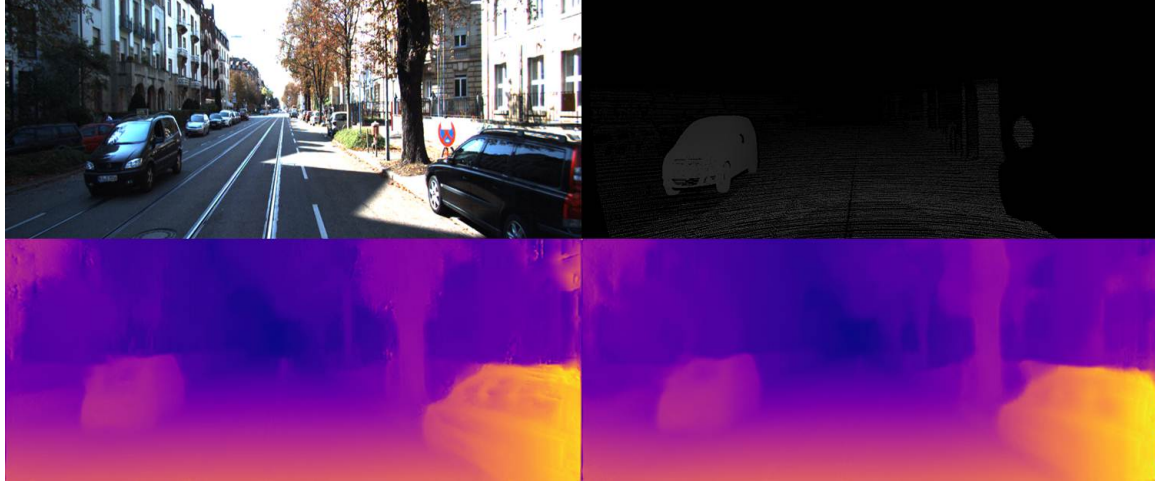


Figure 3. The depth prediction results in form of disparity maps. The input image along with ground truth depth map is shown in 1<sup>st</sup> row taken from KITTI database. The computed disparity maps for DNM6 and DNM12 models are shown in 2<sup>nd</sup> row respectively. Both DNM6 and DNM12 models are capable to detect fine structures such as trees and leaves.

database.

The results comparison of proposed DNM6 and DNM12 models with Godard et al. [8] over Cityscapes database is illustrated in Table 2. In this Table, the training is performed over Cityscapes database, whereas the test images are same as in KITTI database. It is noticed from this experiment that the proposed models are superior than Godard et al. [8] over Cityscapes database in all terms. Moreover, the DNM12 model performs better than DNM6 model. As for as both databases are concerned, the results of proposed models over KITTI database is better than the Cityscapes database. The possible reason can be the difference between the camera calibration between training and testing databases. The similar observations are also made by Godard et al. [8]. The post-processing step enhances the performance of proposed DNM6 and DNM12 models over Cityscapes database.

The qualitative results in terms of the computed disparity maps using DNM6 and DNM12 models are shown in Figure 3 for an input image of driving scene along with its depth map taken from KITTI database. The input image is displayed in 1<sup>st</sup> row and 1<sup>st</sup> column and the ground truth depth map is shown in 1<sup>st</sup> row and 2<sup>nd</sup> column. The computed disparity maps are exhibited in 2<sup>nd</sup> row using DNM6 model in 1<sup>st</sup> column and DNM12 model in 2<sup>nd</sup> column. The disparities generated in this result using proposed methods are able to capture very fine details such as tree at far as well as leaves area which depicts the suitability of dual CNN models.

From the experimental results as shown in Table 1, Table 2 and Figure 3, it is clear that by using dual CNN to train both the stereo images (i.e. left image through left CNN-L and right image through right CNN-R) in fully unsupervised manner, the disparity differences can be minimized

which leads to more generalized and accurate training such that more meaningful depth maps can be generated for test images.

## 5. Conclusions

The supervised depth estimation techniques need the huge amount of training data along with ground truth labels which might not be feasible in real scenario to collect. In this paper, the dual CNN based models are presented for unsupervised monocular depth estimation. Two dual network models DNM6 and DNM12 are proposed based on the number of losses used. The dual network models used two different CNNs (CNN-L and CNN-R) for left and right images of training stereo pairs respectively. In DNM6, total 6 losses including two appearance matching losses, two disparity smoothness losses and two left-right consistency losses are computed. The DNM12 model used the left-right cross mapping i.e. generating left and right disparities from both left and right CNNs, thus doubled the number of losses to 12. The benchmark KITTI driving and Cityscapes urban databases are used for the unsupervised depth estimation experiments. The results are computed in terms of the widely adapted evaluation metrics such as absolute relative differences, RMSE, accuracy etc. The results are also compared with the recent left-right consistency based method. It is observed that the DNM12 outperforms the existing method left-right consistency method. It is also observed that the DNM12 model improves the performance over DNM6 model in most of the cases. The post-processing step further boosts the performance of proposed DNM6 and DNM12 models. The improved results using proposed models confirm the suitability of dual CNN concept to solve the unsupervised depth estimation.

## References

- [1] A. Babenko, A. Slesarev, A. Chigorin, and V. Lempitsky. Neural codes for image retrieval. In *European conference on computer vision*, pages 584–599. Springer, 2014.
- [2] Y. Cao, Z. Wu, and C. Shen. Estimating depth from monocular images as classification using deep fully convolutional residual networks. *IEEE Transactions on Circuits and Systems for Video Technology*, 2017.
- [3] M. Cordts, M. Omran, S. Ramos, T. Rehfeld, M. Enzweiler, R. Benenson, U. Franke, S. Roth, and B. Schiele. The cityscapes dataset for semantic urban scene understanding. In *Proceedings of the IEEE conference on computer vision and pattern recognition*, pages 3213–3223, 2016.
- [4] D. Eigen, C. Puhrsch, and R. Fergus. Depth map prediction from a single image using a multi-scale deep network. In *Advances in neural information processing systems*, pages 2366–2374, 2014.
- [5] Y. Furukawa, B. Curless, S. M. Seitz, and R. Szeliski. Towards internet-scale multi-view stereo. In *Computer Vision and Pattern Recognition (CVPR), 2010 IEEE Conference on*, pages 1434–1441. IEEE, 2010.
- [6] R. Garg, V. K. BG, G. Carneiro, and I. Reid. Unsupervised cnn for single view depth estimation: Geometry to the rescue. In *European Conference on Computer Vision*, pages 740–756. Springer, 2016.
- [7] A. Geiger, P. Lenz, and R. Urtasun. Are we ready for autonomous driving? the kitti vision benchmark suite. In *Computer Vision and Pattern Recognition (CVPR), 2012 IEEE Conference on*, pages 3354–3361. IEEE, 2012.
- [8] C. Godard, O. Mac Aodha, and G. J. Brostow. Unsupervised monocular depth estimation with left-right consistency. In *CVPR*, volume 2, page 7, 2017.
- [9] M. Goesele, N. Snavely, B. Curless, H. Hoppe, and S. M. Seitz. Multi-view stereo for community photo collections. In *Computer Vision, 2007. ICCV 2007. IEEE 11th International Conference on*, pages 1–8. IEEE, 2007.
- [10] R. Hartley and A. Zisserman. *Multiple view geometry in computer vision*. Cambridge university press, 2003.
- [11] K. He, G. Gkioxari, P. Dollár, and R. Girshick. Mask r-cnn. In *Computer Vision (ICCV), 2017 IEEE International Conference on*, pages 2980–2988. IEEE, 2017.
- [12] M. Jaderberg, K. Simonyan, A. Zisserman, et al. Spatial transformer networks. In *Advances in neural information processing systems*, pages 2017–2025, 2015.
- [13] A. Kendall, H. Martirosyan, S. Dasgupta, P. Henry, R. Kennedy, A. Bachrach, and A. Bry. End-to-end learning of geometry and context for deep stereo regression. *CoRR*, vol. abs/1703.04309, 2017.
- [14] H. S. Koppula and A. Saxena. Anticipating human activities using object affordances for reactive robotic response. *IEEE transactions on pattern analysis and machine intelligence*, 38(1):14–29, 2016.
- [15] A. Krizhevsky, I. Sutskever, and G. E. Hinton. Imagenet classification with deep convolutional neural networks. In *Advances in neural information processing systems*, pages 1097–1105, 2012.
- [16] Y. Kuznetsov, J. Stückler, and B. Leibe. Semi-supervised deep learning for monocular depth map prediction. In *Proc. of the IEEE Conference on Computer Vision and Pattern Recognition*, pages 6647–6655, 2017.
- [17] L. Ladicky, J. Shi, and M. Pollefeys. Pulling things out of perspective. In *Proceedings of the IEEE Conference on Computer Vision and Pattern Recognition*, pages 89–96, 2014.
- [18] I. Laina, C. Rupprecht, V. Belagiannis, F. Tombari, and N. Navab. Deeper depth prediction with fully convolutional residual networks. In *3D Vision (3DV), 2016 Fourth International Conference on*, pages 239–248. IEEE, 2016.
- [19] I. Lenz, H. Lee, and A. Saxena. Deep learning for detecting robotic grasps. *The International Journal of Robotics Research*, 34(4-5):705–724, 2015.
- [20] J. Levinson, J. Askeland, J. Becker, J. Dolson, D. Held, S. Kammler, J. Z. Kolter, D. Langer, O. Pink, V. Pratt, et al. Towards fully autonomous driving: Systems and algorithms. In *Intelligent Vehicles Symposium (IV), 2011 IEEE*, pages 163–168. IEEE, 2011.
- [21] B. Li, C. Shen, Y. Dai, A. van den Hengel, and M. He. Depth and surface normal estimation from monocular images using regression on deep features and hierarchical crfs. In *Proceedings of the IEEE Conference on Computer Vision and Pattern Recognition*, pages 1119–1127, 2015.
- [22] B. Liu, S. Gould, and D. Koller. Single image depth estimation from predicted semantic labels. In *Computer Vision and Pattern Recognition (CVPR), 2010 IEEE Conference on*, pages 1253–1260. IEEE, 2010.
- [23] F. Liu, C. Shen, G. Lin, and I. Reid. Learning depth from single monocular images using deep convolutional neural fields. *IEEE transactions on pattern analysis and machine intelligence*, 38(10):2024–2039, 2016.
- [24] W. Luo, A. G. Schwing, and R. Urtasun. Efficient deep learning for stereo matching. In *Proceedings of the IEEE Conference on Computer Vision and Pattern Recognition*, pages 5695–5703, 2016.
- [25] R. Mahjourian, M. Wicke, and A. Angelova. Unsupervised learning of depth and ego-motion from monocular video using 3d geometric constraints. *arXiv preprint arXiv:1802.05522*, 2018.
- [26] J. Michels, A. Saxena, and A. Y. Ng. High speed obstacle avoidance using monocular vision and reinforcement learning. In *Proceedings of the 22nd international conference on Machine learning*, pages 593–600. ACM, 2005.
- [27] D. Nistér. Preemptive ransac for live structure and motion estimation. *Machine Vision and Applications*, 16(5):321–329, 2005.
- [28] P. Rajpurkar, J. Irvin, K. Zhu, B. Yang, H. Mehta, T. Duan, D. Ding, A. Bagul, C. Langlotz, K. Shpanskaya, et al. Chexnet: Radiologist-level pneumonia detection on chest x-rays with deep learning. *arXiv preprint arXiv:1711.05225*, 2017.
- [29] S. Ren, K. He, R. Girshick, and J. Sun. Faster r-cnn: Towards real-time object detection with region proposal networks. In *Advances in neural information processing systems*, pages 91–99, 2015.

- [30] A. Saxena, S. H. Chung, and A. Y. Ng. Learning depth from single monocular images. In *Advances in neural information processing systems*, pages 1161–1168, 2006.
- [31] A. Saxena, S. H. Chung, and A. Y. Ng. 3-d depth reconstruction from a single still image. *International journal of computer vision*, 76(1):53–69, 2008.
- [32] A. Saxena, J. Schulte, A. Y. Ng, et al. Depth estimation using monocular and stereo cues. In *IJCAI*, volume 7, 2007.
- [33] S. M. Seitz, B. Curless, J. Diebel, D. Scharstein, and R. Szeliski. A comparison and evaluation of multi-view stereo reconstruction algorithms. In *Computer vision and pattern recognition, 2006 IEEE Computer Society Conference on*, volume 1, pages 519–528. IEEE, 2006.
- [34] J. Shotton, A. Fitzgibbon, M. Cook, T. Sharp, M. Finocchio, R. Moore, A. Kipman, and A. Blake. Real-time human pose recognition in parts from single depth images. In *Computer Vision and Pattern Recognition (CVPR), 2011 IEEE Conference on*, pages 1297–1304. Ieee, 2011.
- [35] K. Simonyan and A. Zisserman. Very deep convolutional networks for large-scale image recognition. *arXiv preprint arXiv:1409.1556*, 2014.
- [36] D. Stoyanov, M. V. Scarzanella, P. Pratt, and G.-Z. Yang. Real-time stereo reconstruction in robotically assisted minimally invasive surgery. In *International Conference on Medical Image Computing and Computer-Assisted Intervention*, pages 275–282. Springer, 2010.
- [37] A. Torralba and A. Oliva. Depth estimation from image structure. *IEEE Transactions on pattern analysis and machine intelligence*, 24(9):1226–1238, 2002.
- [38] Z. Wang, A. C. Bovik, H. R. Sheikh, and E. P. Simoncelli. Image quality assessment: from error visibility to structural similarity. *IEEE transactions on image processing*, 13(4):600–612, 2004.
- [39] C. Wu. Towards linear-time incremental structure from motion. In *3D Vision-3DV 2013, 2013 International conference on*, pages 127–134. IEEE, 2013.
- [40] J. Xie, R. Girshick, and A. Farhadi. Deep3d: Fully automatic 2d-to-3d video conversion with deep convolutional neural networks. In *European Conference on Computer Vision*, pages 842–857. Springer, 2016.
- [41] D. Xu, E. Ricci, W. Ouyang, X. Wang, and N. Sebe. Multi-scale continuous crfs as sequential deep networks for monocular depth estimation. In *Proceedings of CVPR*, 2017.
- [42] J. Zbontar and Y. LeCun. Stereo matching by training a convolutional neural network to compare image patches. *Journal of Machine Learning Research*, 17(1-32):2, 2016.
- [43] T. Zhou, M. Brown, N. Snavely, and D. G. Lowe. Unsupervised learning of depth and ego-motion from video. In *CVPR*, volume 2, page 7, 2017.
- [44] T. Zhou, P. Krahenbuhl, M. Aubry, Q. Huang, and A. A. Efros. Learning dense correspondence via 3d-guided cycle consistency. In *Proceedings of the IEEE Conference on Computer Vision and Pattern Recognition*, pages 117–126, 2016.